Analyst

Accepted Manuscript

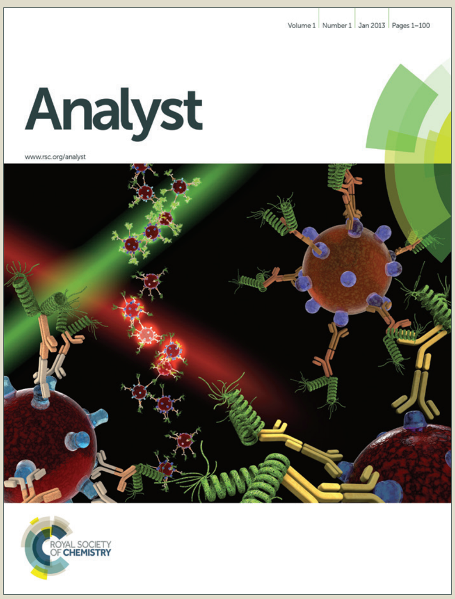

MnO_2 Nanosheets Based Fluorescent Sensing Platform with Organic Dyes as Probe with Excellent Analytical Properties

Chunxia Wang, Wanying Zhai, Yuexiang Wang, Ping Yu, and Lanqun Mao*

Beijing National Laboratory for Molecular Sciences, Key Laboratory of Analytical Chemistry for Living Biosystems, Institute of Chemistry, the Chinese Academy of Sciences, Beijing 100190, China.

* Corresponding author. Fax: +86-10-62559373, E-mail: lqmao@iccas.ac.cn.

Abstract

Manganese dioxide (MnO_2) nanosheets have recently been demonstrated to be particularly attractive for fluorescent sensing and imaging, however, almost all MnO_2 nanosheets-based fluorescent assays have been developed with emissive nanoparticles as the probes. In this study, we developed a novel strategy to use organic dyes, instead of emissive nanoparticles as the probe, to construct a platform for biosensing with excellent analytical properties. With 5-carboxyfluorescein (FAM) as a model organic dye, we firstly investigate the effect of MnO_2 nanosheets on the fluorescence of FAM and find that the fluorescent intensity of FAM is considerably suppressed by MnO_2 nanosheets based on the inner filter effect (IFE). To demonstrate the MnO_2 nanosheets-based fluorescence sensing platform can easily achieve a high selectivity with organic dyes as the probe, we use single-stranded DNA (ssDNA) oligonucleotide as a typical biorecognition unit, on which FAM probe is labeled to form FAM-ssDNA. The fluorescent intensity of FAM-ssDNA is first suppressed by MnO_2 nanosheets through the combination of IFE and Förster resonant energy transfer (FRET), and then recovered with the subsequent hybridization with complementary DNA oligonucleotide. To demonstrate the potential applications of MnO_2 nanosheets-based fluorescence sensing platform with organic dyes as the probes, we develop the methods for simple but effective microRNA and thrombin assays. With the platform demonstrated here, the limits of detection for miR124a and thrombin are down to 0.8 nM and 11 nM, respectively. Moreover, the fluorescent sensing assay of thrombin exhibits a high selectivity. This study essentially demonstrates a new 2D nanostructure-based fluorescent sensing platform, which is robust, technically simple, and easily manipulated to have high selectivity and sensitivity for practical applications.

Introduction

Recent rapid development of two-dimensional (2D) nanostructures has greatly evoked extensive research interests from analytical chemistry community, fluorescence assays in particular, because these materials can be used as one of the most promising quenchers with high fluorescent quenching efficiency and good aqueous solubility to constitute new fluorescent sensing mechanisms with excellent analytical properties.[1-5] As a typical example, the one-atomic-thick carbon nanosheet graphene has been widely used to develop analytical platforms for fluorescence sensing of a large variety of targets including metal ions, small molecules, proteins and DNA, owing to its high fluorescence quenching ability.[6-10] Besides, other kinds of 2D nanosheets composed of various materials including transition-metal dichalcogenides, transition metal oxides, and C_3N_4 have also been demonstrated to be particularly useful for fluorescence sensing applications.[3, 4, 11]

Manganese dioxide (MnO_2) nanosheets are one kind of 2D nanomaterials with the thickness of nanometers or even smaller while the lateral size ranges from submicrometers to micrometers.[12-14] MnO_2 nanosheets have received much attention in terms of their potential applications in electrochemistry, catalysis, energy conversion and storage.[15-17] Recent attempts have demonstrated MnO_2 nanosheets are particularly useful for fluorescent sensing and bio-imaging owing to their wide absorption band, redox activity, and good biocompatibility.[18-21] For example, MnO_2 nanosheets have been used as a nanoquencher towards upconversion nanoparticles and luminescent nanomaterials and, based on this mechanism, they can be used for fluorescence sensing and bioimaging.[18-20] Very recently, Tan et al. reported a dual bimodal detection with fluorescence/MRI for tumor cell imaging by taking advantage of the redox activity and light absorbing property of MnO_2 nanosheets.[1]

Despite of the enormous works dedicated to the combination of emissive nanoparticles and MnO_2 nanosheets, our recent investigation demonstrated a novel approach of MnO_2

nanosheets-based fluorescent assays with organic dyes, rather than emissive nanoparticles, as the probes.[21] We have been particularly interested in this strategy because first, MnO_2 nanosheets have rich surface chemistry, which enables various interactions with different kinds of organic dyes and, as a consequence, triggers the change in the fluorescence of the dyes through multiple and even tailor-made mechanisms. Second, organic dyes with functional moieties could be easily integrated with recognition elements and, as a result, the selectivity toward the targets could be readily achieved through binding/labeling the dyes onto the recognition elements.[22-23] This is remarkable because the MnO_2 nanosheets-based fluorescent methods reported so far mostly rely on the redox property of MnO_2 nanosheets themselves and/or the uses of enzymes to achieve the selectivity, which are technically complicated and less cost-effective.[1,18-21] Third, benefited from the good solubility of organic dyes in aqueous solutions, this platform bears technically simplicity with robust analytical properties, with few requirements employed for carefully manipulating the distance between nanoparticles and MnO_2 nanosheets to tune the efficiency of Förster resonant energy transfer (FRET) when luminescent nanoparticles are used as fluorescence probes.[20,24] In spite of these advantages, the potentiality of the uses of organic dyes as the probes to establish a MnO_2 nanosheets-based fluorescence sensing platform remains to be further explored.

In this study, we demonstrate a MnO_2 nanosheets-based fluorescence sensing platform with organic dyes, rather than emissive nanostructures, as the probes, by using 5-carboxyfluorescein (FAM) as a model organic dye. We find that the fluorescence intensity of FAM decreases with increasing the concentration of MnO_2 nanosheets into the solution mainly through the inner filter effect (IFE) of MnO_2 nanosheets. To demonstrate the advantage of the organic dye-based sensing platform in simply achieving the selectivity toward the targets, we use DNA as the model biorecognition elements to constitute selective fluorescence assays, in which the organic dye (i.e., FAM) is labeled on the single-stranded

DNA (ssDNA) oligonucleotides to form FAM-ssDNA (Scheme 1). Similar to that of FAM, the fluorescence intensity of FAM-ssDNA is effectively suppressed by MnO_2 nanosheets through the combination of IFE and Förster resonant energy transfer (FRET). Based on this, a fluorescence sensing platform can be developed for various targets such as microRNA (miRNA) and thrombin with high selectivity and reliability through the fluorescence suppression of FAM-ssDNA with MnO_2 nanosheets and fluorescence recovery with the presence of the targets as the signal readout (Scheme 1). This study essentially demonstrates a new MnO_2 nanosheets-based fluorescence sensing platform with organic dyes as the probes with easily manipulated analytical properties.

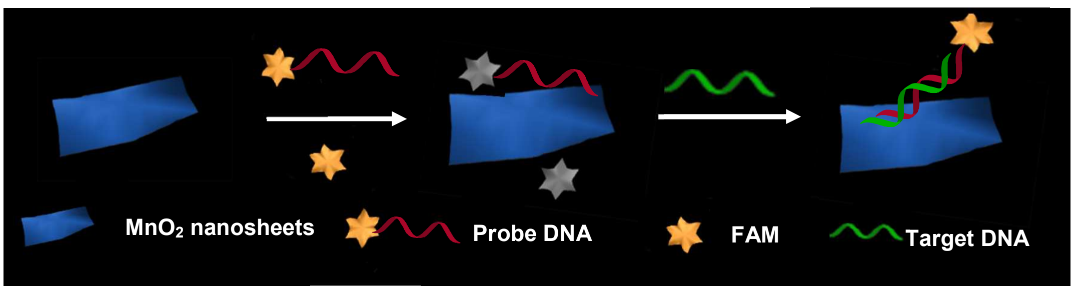

Scheme 1. Schematic illustration of MnO_2 nanosheets-based fluorescence sensing platform with FAM as the probe.

Experimental

Chemicals and reagents

All of the DNA and RNA oligonucleotides used in this study (Table S1) were synthesized and purified by Invitrogen Inc. (Beijing, China) and Takara biotechnology (Dalian, China), respectively. $MnCl_2$•$4H_2O$ were purchased from Beijing Chemical Company (Beijing, China). Tetramethylammonium hydroxide (TMA•OH) was obtained from Alfa Aesar Inc. (Shanghai, China). 5-Carboxyfluorescein (FAM) and BSA was purchased from Sigma-Aldrich (Shanghai, China). HEPES buffer (10 mM, containing 75 mM NaCl, and 4.0 mM $MgCl_2$, pH 7.5) was used for DNA, miRNA and thrombin assays. Aqueous solutions were prepared with Milli-Q water (≥18.2 MΩ cm).

Preparation of MnO_2 nanosheets

MnO_2 nanosheets were synthesized as reported previously.[14] Briefly, 20 mL of aqueous solution containing 12 mM tetramethylammonium hydroxide (TMA•OH) was mixed with 2 mL of H_2O_2 (3.0 wt%). The mixture was added drop by drop into the aqueous solution of $MnCl_2$•$4H_2O$ (0.3 M, 10 mL) within 15 s. The resulting mixture was stirred vigorously overnight in the open air at room temperature to give a dark brown suspension. The suspension was centrifuged and the resulting precipitate was filtrated, sequentially washed with water and methanol, and finally dispersed into water to form a homogenous suspension under sonication. MnO_2 nanosheets prepared here have a size of about 200 nm in lateral width with occasional folds and crinkles (Fig. S1A). The thickness of as-formed MnO_2 nanosheets was about ~ 1.4 nm as characterized by tapping-mode atomic force microscopy (Fig. S1B). Energy dispersive X-ray spectroscopy analysis (Fig. S1C) indicated the presence of Mn and O elements. Zeta potential distribution indicated that MnO_2 nanosheets have a relatively electronegative zeta potential of -29.6 mV (Fig. S1D). The absorption spectrum of MnO_2 nanosheets prepared here exhibit a wide band in the range from 230 nm to 700 nm with an absorption peak at 380 nm (Fig. S1E). The extinction coefficient was calculated to be 9.4×10^{-3} M^{-1} cm^{-1} from the concentration-dependent UV-vis spectrum of MnO_2 nanosheets (Fig. S1F).

Apparatus and fluorescent measurements

Fluorescence experiments were carried out on an F-4600 fluorescence spectrophotometer (Hitachi, Japan) equipped with a Xenon lamp excitation source. UV-vis absorption spectra were recorded on a TU-1900 spectrophotometer (Beijing, China). Transmission electron microscopy (TEM) image was taken on a TEM-2100F microscopy

(JEOL, Japan). Tapping mode atomic force microscopic (AFM) image was acquired on a Vecco Nanoscope III by directly casting the samples onto the surface of mica substrate. Zeta potential distribution was recorded on a Zetasizer (Nano-Z, Malvern, UK).

For the mechanistic investigation on the effects of MnO_2 nanosheets on the fluorescence of free FAM, FAM-T15, and FAM-T15/A15, we separately added 60 μL of aqueous dispersion of MnO_2 nanosheets with various concentrations (0, 4, 10, 20, 30, 40, 50, 60, 80, and 100 μM) into the aqueous solutions of FAM (25 μL, 40 nM), FAM-T15 (5'-FAM-TTTTTTTTTTTTTTT-3'; 20 μL, 40 nM), and FAM-T15/A15 formed by hybridization of FAM-T15 (20 μL, 40 nM) with A15 (5'-AAAAAAAAAAAAAAA-3'; 40 μL, 80 nM) at 55°C in water bath for 10 min in 2.5 mL HEPES buffer. The resulting mixtures were allowed to stand by for 5 min prior to the recording of UV-vis and fluorescence spectra. In the fluorescence anisotropy experiments, FAM-T15 (2 μL, 20 nM) and the aqueous dispersion of MnO_2 nanosheets (60 μL, 60 μM) were mixed into 1 mL HEPES buffer, in which A15 (10 μL, 100 nM) was mixed. The resulting mixture was incubated at 55°C in water bath for 10 min and then gradually cooled to room temperature. The mixture was allowed to stand by for 5 min prior to the fluorescence measurements.

Fluorescent miRNA assays

To demonstrate the applications of the MnO_2 nanosheets-based fluorescence sensing platform with organic dyes as the probes, as a first example, we demonstrate the application of such a platform for selective miRNA sensing. For this purpose, FAM dye was labeled onto specific probe sequence (i.e., 5'-GGCATTCACCGCGTGCCTTA-3') to form 5'-FAM-GGCATTCACCGCGTGCCTTA-3' (FAM-PmiR). In a typical procedure, 2 μL of FAM-PmiR (20 nM) was mixed with different concentrations of target miR124a (i.e., 5'-UAAGGCACGCGGUGAAUGCC-3') (0.0, 2.0, 4.0, 8.0, 12, 16, 20, 30, 50, and 80 nM) dissolved in 1 mL HEPES buffer. The mixtures were then incubated at 55 °C for 10 min and gradually cooled to room temperature. After that, 60 μL of aqueous dispersion of MnO_2 nanosheets (60 μM) was added into each mixture and the resulting mixtures were then allowed to stand by for 5 min prior to the fluorescence measurements.

Fluorescent thrombin assays

Fluorescent thrombin assay was used as the other example to demonstrate the application of the MnO_2 nanosheets-based fluorescence sensing platform with organic dyes as the probes. Similar to the strategy employed for miRNA sensing, FAM was labeled onto thrombin binding aptamer (TBA) to form 5'-FAM-GGTTGGTGTGGTTGG-3' (FAM-TBA). A 4 μL of FAM-TBA (40 nM) in 1 mL HEPES buffer was mixed with different concentrations of thrombin (0, 20, 40, 60, 80, 100, 120, 140, 160, 200, 250, 300, 500, 1500, 3000, 5000, 7500, and 10000 nM), and the mixtures were incubated at 55 °C for 10 min. After that, an aliquot of MnO_2 nanosheets (60 μL, 60 μM) was added to the mixtures and the resulting mixtures were allowed to stand by for 5 min prior to the fluorescence measurements.

Results and discussion

Suppressive effect of MnO_2 nanosheets toward fluorescence of FAM and FAM-ssDNA

As depicted in Fig. 1A, FAM exhibits an emission band with a maximum emission at 522 nm with an excitation wavelength at 490 nm (red curve). MnO_2 has an intense and broad absorption ranging from 200 nm to 600 nm (blue curve), which overlaps with the excitation and emission of FAM (black and red curves). The fluorescence intensity of FAM decreases with increasing the concentration of MnO_2 nanosheets in the solution (Fig. 1B). The MnO_2 nanosheets-induced fluorescence suppression of FAM was considered to arise from inner filter effect (IFE) in terms of the overlapping between the spectrum of MnO_2 nanosheets and the excitation/emission spectra of FAM (Fig. 1A). To further investigate the IFE on the MnO_2 nanosheets-induced fluorescent suppression, IFE was corrected on the basis of the cell geometry (Fig. S2) and the absorption characteristics of aqueous solution of MnO_2 nanosheets and FAM with equation 1.[25]

$$\frac{F_{cor}}{F_{obsd}} = \frac{2.3dA_{ex}}{1-10^{-dA_{ex}}} 10^{gA_{em}} \frac{2.3sA_{em}}{1-10^{-sA_{em}}} \qquad (1)$$

Where, F_{obsd} refers to the observed fluorescence intensity, and F_{cor} is the corrected fluorescence intensity by removing IFE from F_{obsd} (λ_{em} = 522 nm); A_{ex} and A_{em} represent the absorbance at the excitation wavelength (λ_{ex} = 490 nm) and emission wavelength (λ_{em} = 522 nm), respectively; s is the thickness of excitation beam (i.e., 0.10 cm in this study), g is the fixed distance from the edge of the excitation beam to the edge of the cuvette (i.e., 0.40 cm in this case), and d is the width of the cuvette (i.e., 1.00 cm in this case).

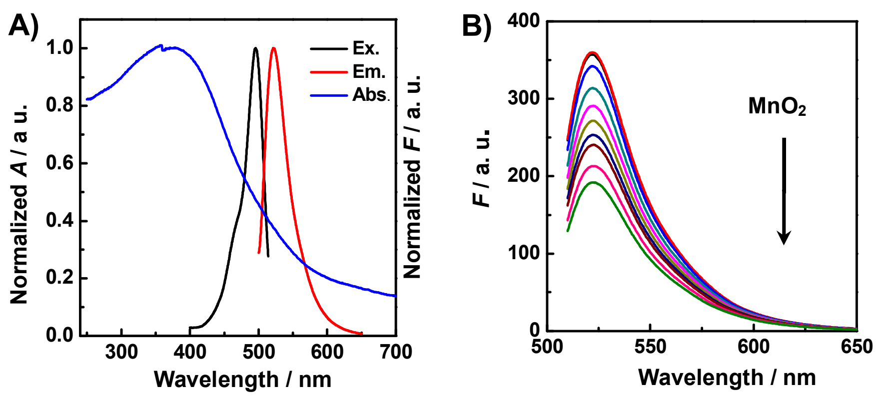

Fig. 1 (A) Normalized fluorescence excitation spectrum (black curve) and emission spectrum (red curve) of FAM and normalized UV-vis absorption spectra of MnO_2 nanosheets (blue curve). (B) Fluorescence spectra of FAM (25 μL, 40 nM) upon addition of various concentrations of MnO_2 nanosheets (from upper to bottom: 0.0, 4.0, 10, 20, 30, 40, 50, 60, 80, and 100 μM). Excitation wavelength, 490 nm.

Table 1 summarizes the concentrations of MnO_2 nanosheets, absorbance and fluorescence intensity of FAM after adding different concentrations of MnO_2 nanosheets. The correction factor (*CF*) of IFE at each concentration of MnO_2 nanosheets shown in Table 1 was generated from the equation 1. Fig. 2 demonstrates the observed (E_{obsd}, black dots) and corrected fluorescence efficiency (E_{cor}, red dots, after subtracting the IFE from the observed fluorescence) in the absence and presence of MnO_2 nanosheets, from which we found that the maximum suppressed efficiency of IFE for MnO_2 nanosheets towards FAM was as high as 90% of total suppressed efficiency, suggesting the suppressive effect mainly come from

Table 1. Parameters Used to Calculate IFE of MnO_2 Nanosheets on the Fluorescence of FAM

MnO_2 (μM)	A_{ex} [a]	A_{em} [b]	CF [c]	F_{obsd} [d]	F_{cor} [e]	E_{obsd} [f]	E_{cor} [g]
0	0.022	0.005	1.028	355.0	365.1	0	0
4	0.041	0.019	1.066	340.1	362.7	0.0419	0.0065
10	0.063	0.037	1.113	321.7	358.3	0.0938	0.0186
20	0.116	0.074	1.227	293.6	360.4	0.1729	0.0128
30	0.160	0.107	1.332	268.8	358.2	0.2428	0.0188
40	0.202	0.138	1.439	243.8	350.9	0.3132	0.0388
50	0.240	0.167	1.543	229.9	354.9	0.3523	0.0279
60	0.275	0.194	1.646	214.0	352.3	0.3971	0.0350
80	0.335	0.240	1.835	189.0	346.9	0.4676	0.0498
100	0.394	0.287	2.043	167.8	342.8	0.5273	0.0610

[a] A_{ex} is the absorbance of FAM with the addition of MnO_2 nanosheets at 490 nm. [b]A_{em} is the absorbance of FAM with the addition of MnO_2 nanosheets at 522 nm. [c] Corrected factor (*CF*) was calculated as F_{cor}/F_{obsd}. [d] F_{obsd} is the measured fluorescence intensity of FAM with the addition of MnO_2 nanosheets at 522 nm. [e] F_{cor} is the corrected fluorescence intensity with eq.1 by removing IFE from the measured fluorescence intensity (i.e., F_{obsd}). [f] $E_{obsd} = 1\text{-}F_{obsd}/F_{obsd,0}$. $F_{obsd,0}$ and F_{obsd} are the observed fluorescence intensities of FAM in the absence and presence of MnO_2 nanosheets, respectively. [g] $E_{cor} = 1\text{-}F_{cor}/F_{cor,0}$. $F_{cor,0}$ and F_{cor} are the corrected fluorescence intensities of FAM in the absence and presence of MnO_2 nanosheets, respectively.

IFE. This is relatively different from those employed for other kinds of nanomaterials, which were mainly based on FRET or photo induced electron transfer (PET).[10,11,26] This mechanism is essentially stemmed from the unique optical property of MnO_2 nanosheets; their wide absorption band almost covers the whole absorption spectrum, which well overlaps the spectra of various organic dyes and thus readily induces IFE.

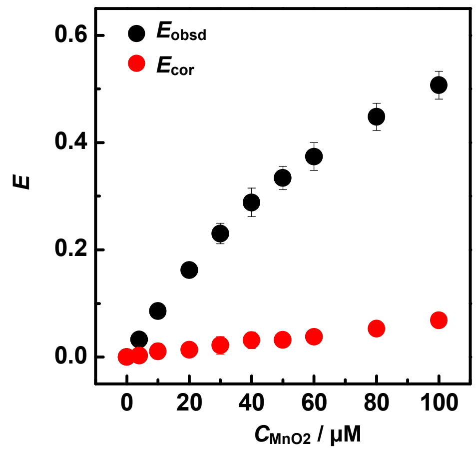

Fig. 2 Observed (black dots, E_{obsd}) and corrected (red dots, E_{cor}) suppressed efficiency of MnO_2 nanosheets towards FAM (25 μL, 40 nM) with addition of various concentrations of MnO_2 nanosheets (0.0, 4.0, 10, 20, 30, 40, 50, 60, 80, and 100 μM). $E = 1\text{-}F/F_0$. F_0 and F are the fluorescence intensities of FAM in the absence and presence of MnO_2 nanosheets, respectively. Excitation wavelength, 490 nm. Emission wavelength, 522 nm. Error bars were the standard deviation of three independent experiments.

In our early study, by taking advantage of the broad absorption band and the redox property of MnO_2 nanosheets, we have developed an in vivo sensing strategy for ascorbic acid based on the suppressive effect of MnO_2 nanosheets on the fluorescence of 7-hydroxycoumarin and the restoration of the fluorescence with ascorbic acid through the redox reaction between ascorbic acid and MnO_2 nanosheets.[21] In that case, the selectivity was achieved by fully taking advantages of redox property of MnO_2 nanosheets and the use of ascorbate oxidase. As demonstrated below, the use of organic dyes as the probes would largely enable the selectivity to be achieved in a simple way since the dyes themselves bear, or can be rationally designed to have, functional moieties that enable the dyes to be readily integrated onto the recognition elements such as aptamers,[3,9,27] nucleic acids,[10,28-31] and peptide nucleic acid[32] for selective fluorescence sensing.

To demonstrate the strategy through the use of organic dyes as the probes to readily achieve the selectivity for the as-established MnO_2 nanosheets-based fluorescence sensing platform, we used DNA oligonucleotides as a model recognition element. In this case, FAM was labeled onto the single stranded DNA oligonucleotides (T15, 5'-FAM-TTTTTTTTTTTTTTT-3') to form FAM-T15, and the effect of MnO_2 nanosheets on the fluorescence of FAM-T15 was then investigated. Similar to those observed for free FAM, the addition of increasing concentrations of MnO_2 nanosheets clearly results in the decrease in the fluorescence intensity of FAM-T15 (Fig. 3A). As displayed in Fig. 3B, the observed

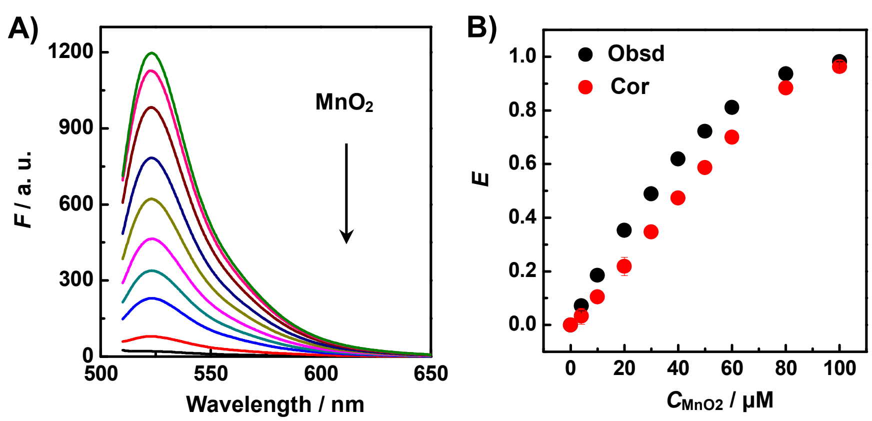

Fig. 3 (A) Fluorescence spectra of FAM-T15 (20 μL, 40 nM) upon addition of various concentrations of MnO_2 nanosheets (from upper to bottom: 0.0, 4.0, 10, 20, 30, 40, 50, 60, 80, and 100 μM). (B) Observed (black dots, E_{obsd}) and corrected (red dots, E_{cor}) suppressed efficiency of MnO_2 nanosheets towards FAM-T15 (20 μL, 40 nM). $E = 1\text{-}F/F_0$. F_0 and F are the fluorescence intensities of FAM-T15 (20 μL, 40 nM) in the absence and presence of MnO_2 nanosheets, respectively. Excitation wavelength, 490 nm. Emission wavelength, 522 nm. Error bars were the standard deviation of three independent experiments.

suppressive efficiency of MnO_2 nanosheets (black dots), which was defined as $E = 1\text{-}F/F_0$ (F_0 and F are the observed fluorescence intensities of FAM-T15 in the absence and presence of MnO_2 nanosheets, respectively), towards the fluorescence of FAM-T15 was higher than that toward the fluorescence of free FAM under the same conditions (Fig. 2, black dots). After removing the IFE from observed suppressive efficiency, we found that the maximum corrected suppressive efficiency (E_{cor}) of MnO_2 nanosheets towards FAM-T15 reaches up to 98%, as depicted in Fig. 3B (red dots, data shown in Table S2), which was much higher than that of free FAM (i.e., only about 10%) (Fig. 2, red dots). In this sense, IFE plays a tiny part in the whole suppressed efficiency of MnO_2 nanosheets towards the fluorescence of FAM-T15. The difference in the mechanism underlying the suppressive effects of MnO_2 nanosheets toward the fluorescence of free FAM and FAM-T15 might be elucidated by the interaction between MnO_2 nanosheets and DNA oligonucleotides that virtually shortens the distance between FAM and nanosheets, resulting in the occurrence of FRET.

To verify the strategy to obtain the selectivity by labeling organic dyes onto DNA oligonucleotides for fluorescence sensing, we first hybridized FAM-T15 with its complementary DNA (i.e., A15) to form labeled double-stranded DNA (i.e., FAM-T15/A15), and then studied the effect of MnO_2 nanosheets on the fluorescence of FAM-T15/A15, as typically shown in Fig. 4A. As shown in Fig. 4B, different suppressed efficiency (E_{obsd}) of MnO_2 nanosheets was obtained toward the fluorescence of FAM-T15 (black dots) and FAM-T15/A15 (red dots). From the observed fluorescence efficiency (E_{obsd}), we found that MnO_2 nanosheets exhibit less suppressive effect on the fluorescence of FAM-T15/A15 (red dots) as compared with that of FAM-T15 (black dots), as depicted in Fig. 4B (data shown in Table S3). After removing the IFE, the corrected suppressed efficiency (E_{cor}, Fig. S3) of MnO_2 nanosheets toward the fluorescence of FAM-T15 (blue dots, Fig. S3) and FAM-T15/A15 (orange dots, Fig. S3) differs greatly, which is consistent with E_{cor} shown in

Fig. 4B. This result suggests that the hybridization of ssDNA oligonucleotides with its complementary DNA sequence could result in the restoration of the MnO_2 nanosheets-suppressed fluorescence of FAM-ssDNA and such a property essentially forms a straightforward basis for selective fluorescence sensing, as demonstrated later.

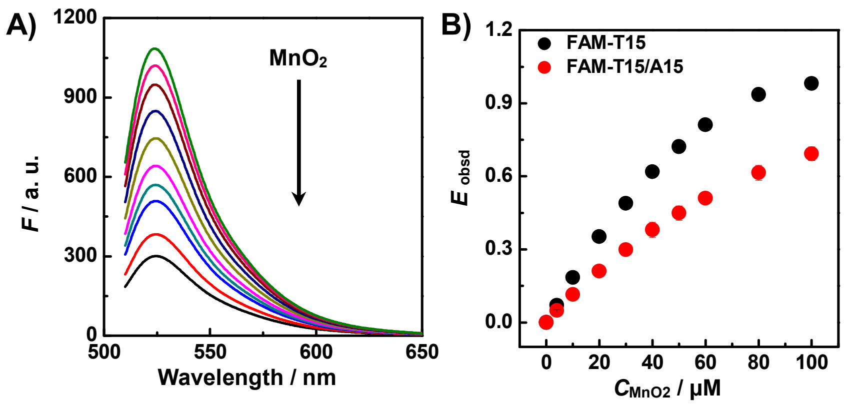

Fig. 4 (A) Fluorescence spectra of FAM-T15 (20 μL, 40 nM) after hybridization with A15 (40 μL, 80 nM) upon the addition of different amounts of MnO_2 nanosheets (from upper to bottom: 0.0, 4.0, 10, 20, 30, 40, 50, 60, 80, and 100 μM). (B) Suppressed efficiency (E = 1-F/F_0) of observed (E_{obsd}) fluorescence of FAM-T15 (20 μL, 40 nM), and FAM-T15 (20 μL, 40 nM) after hybridization with A15 (40 μL, 80 nM) in the absence and presence of MnO_2 nanosheets. F_0 and F are the fluorescence intensities of FAM-T15 (20 μL, 40 nM), and FAM-T15 (20 μL, 40 nM) after hybridization with A15 (40 μL, 80 nM) in the absence and presence of MnO_2 nanosheets, respectively. Excitation wavelength, 490 nm. Emission wavelength, 522 nm. Error bars were the standard deviation of three independent experiments.

To probe the mechanism underlying the fluorescence restoration with hybridization of FAM-ssDNA into FAM-dsDNA, we *in situ* hybridized FAM-T15 with A15 and studied the effect of MnO_2 nanosheets on the fluorescence of the as-formed FAM-T15/A15. Initially, FAM-T15 exhibits strong fluorescence intensity at 522 nm with an excitation at 490 nm (Fig. 5, blue curve). The addition of MnO_2 nanosheets to the solution results in large fluorescence suppression (Fig. 5, red curve). Hybridization of A15 leads to the duplex formation, which

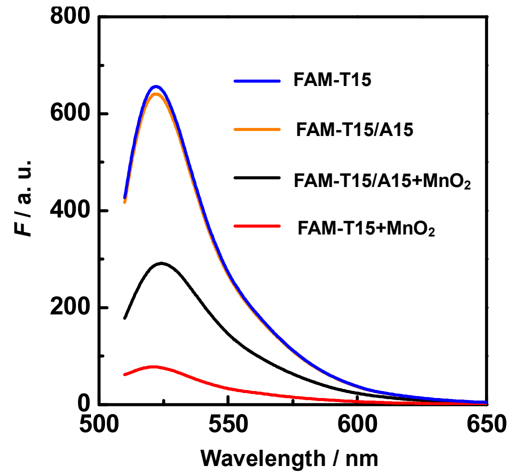

Fig. 5 Fluorescence spectra of FAM-T15 (2 μL, 20 nM, blue curve), FAM-T15 (2 μL, 20 nM) after hybridization with A15 (10 μL, 100 nM, orange dots), FAM-T15 (2 μL, 20 nM) with addition of MnO_2 nanosheets (60 μL, 60 μM) (red curve), and hybridization of A15 (10 μL, 100 nM) with FAM-T15 and MnO_2 nanosheets (black curve). Excitation wavelength, 490 nm. Emission wavelength, 522 nm.

enables the fluorescence restoration (Fig. 5, black curve). The restoration was elucidated in terms of the weaker interaction between FAM-T15/A15 and MnO_2 nanosheets than that between FAM-T15 and MnO_2 nanosheets. This is because the formation of FAM-T15/A15 results in desorption of FAM-T15 from the surface of MnO_2 nanosheets, as illustrated in fluorescence anisotropy (Fig. S4), resulting in the fluorescence restoration. Note that, the fluorescence intensity of FAM-T15/A15 at 522 nm (Fig. 5, orange curve) was very close to that of FAM-T15, suggesting that the introduction of A15 does not lead to great effect on the fluorescence FAM-T15 with the absence of MnO_2 nanosheets, which was consistent with the previous study.[33] The restoration of the fluorescence upon the hybridization of FAM-T15 with its complementary DNA oligonucleotide strongly suggests that the strategy demonstrated here could be developed into a fluorescence sensing platform for practical analytical applications with a high selectivity.

Toward fluorescent sensing application

To demonstrate the possibility that MnO_2 nanosheets might serve as a sensing platform for practical applications, we first explored this sensing platform for selectively monitoring microRNA. MicroRNAs (miRNAs) are short endogenous noncoding RNAs (19-23 nucleotides), which play a critical role in biological processes and could be used for early diagnosis of diseases and discovery of new targets for drugs.[34-40] miR124a (5'-UAAGGCACGCGGUGAAUGCC-3'), the most abundant microRNA expressed in the vertebrate central nervous system (CNS), which is required for hippocampal axogenesis and retinal cone survival through Lhx2 suppression,[41-43] was selected as the target in this case. For the sensing purpose, FAM-PmiR (5'-FAM-GGCATTCACCGCGTGCCTTA-3') was designed to be complementary to miR124a. In a typical experiment, FAM-PmiR (2 μL, 20 nM) was mixed with miR124a at various concentrations and the resulting mixtures were incubated at 55°C for 10 min and then added with an aliquot of MnO_2 nanosheets solution (60 μL, 60 μM) for fluorescence measurements. As shown in Fig. 6A, the increase in the concentrations of miR124a in the hybridization solution leads to an increase of fluorescence intensity. The increase in the fluorescence intensity was linear with the concentration of miR124a within a concentration range from 0 nM to 20 nM ($F/F_0 = 0.116\ C_{\mathrm{miR124a}}/\ \mathrm{nM} + 1.08$, $R^2 = 0.987$) with a limit of detection (LOD) of 0.8 nM (S/N = 3) (Fig. 6B, inset). The LOD for the target was higher than the enzyme-amplified or GO-based fluorescence analysis[44-49] but was comparable to other microRNA detection strategies such as fluorescent ligand-based fluorescence detection.[50]

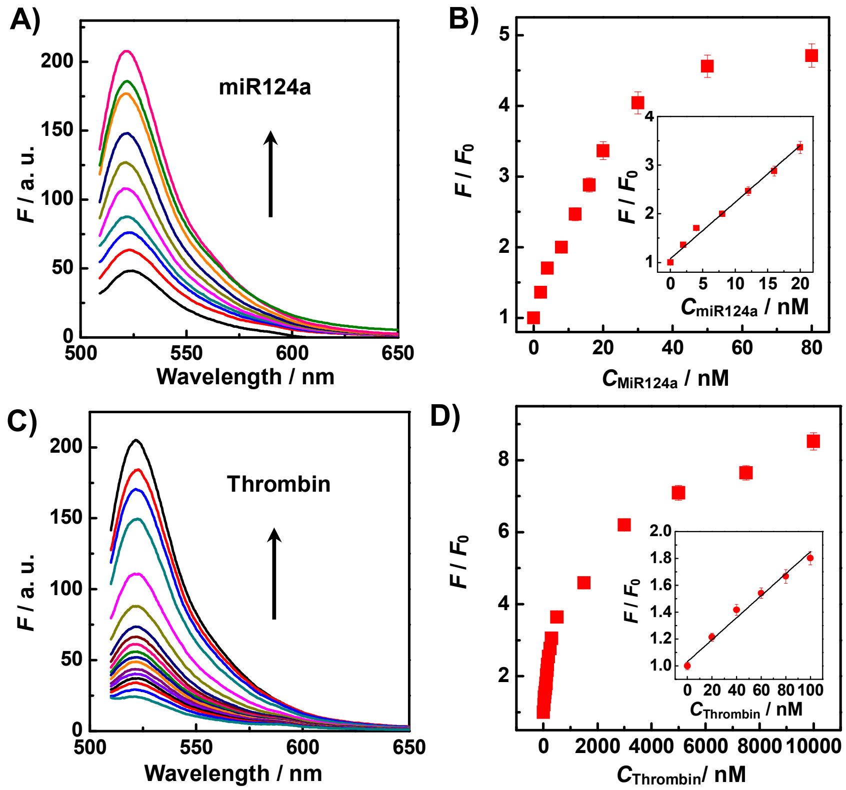

Fig. 6 (A) Fluorescence spectra of FAM-PmiR (2 μL, 20 nM) after hybridization with different concentrations of miR124a (from bottom to top: 0.0, 2.0, 4.0, 8.0, 12, 16, 20, 30, 50, and 80 nM) with the addition of MnO_2 nanosheets (60 μL, 60 μM). (B) Plot of F/F_0 versus the concentration of miR124a. Inset, calibration curve. F_0 and F denote the fluorescence intensities of FAM-PmiR (2 μL, 20 nM) and MnO_2 nanosheets (60 μL, 60 μM) before and after the hybridization of FAM-PmiR with miR124a, respectively. (C) Fluorescence spectra of FAM-TBA (4 μL, 40 nM) after incubation of FAM-TBA with different concentrations of thrombin (from bottom to top: 0, 20, 40, 60, 80, 100, 120, 140, 160, 200, 250, 300, 500, 1500, 3000, 5000, 7500, and 10000 nM) with the addition of MnO_2 nanosheets (60 μL, 60 μM). (D) Plot of F/F_0 versus the concentration of thrombin. Inset, calibration curve. F_0 and F denote the intensities of FAM-TBA (4 μL, 40 nM) and MnO_2 nanosheets (60 μL, 60 μM) before and after incubation of FAM-TBA with thrombin, respectively. Excitation wavelength, 490 nm. Emission wavelength, 522 nm. Error bars were the standard deviation of three independent experiments.

As the other example to demonstrate the application of MnO_2 nanosheets fluorescence sensing platform with organic dyes as the probes and with DNA as the recognition elements, selective sensing of thrombin was illustrated by the following experiments. As reported previously, molecular recognition strategy with aptamers as the recognition element has been widely used for sensing applications, ranging from small molecules, proteins, and even cells.[51-53,1] Herein, as a proof of concept experiment, FAM probe was labeled onto thrombin binding aptamer (TBA, 5'-GGTTGGTGTGGTTGG-3') to form FAM-TBA (5'-FAM-GGTTGGTGTGGTTGG-3') and the fluorescence measurements were carried out.

Fig. 6C depicts the fluorescence emission of FAM-TBA after FAM-TBA was incubated with various concentrations of thrombin and then mixed with an aliquot of MnO_2 nanosheets dispersion. As expected, the fluorescence intensity of FAM-TBA was intensified with increasing the concentration of thrombin in the hybridization solution. As depicted in Fig. 6D, the enhanced fluorescence intensity increases with increasing the concentration of thrombin and was linear with the concentration of thrombin within a concentration range from 0 to 100 nM (F/F_0 = 0.008 C_{thrombin}/ nM + 1.05, R^2 = 0.980). The LOD was calculated to be as 11 nM (S/N = 3) (Fig. 6D, inset), which was comparable to the existing graphene-based strategy.[9] These results demonstrate that this strategy can be used as a sensing platform for thrombin detection. Moreover, the method demonstrated here also displays a high selectivity towards thrombin over the other species (Fig. S5), demonstrating that the platform developed here could be used for practical applications.

Conclusions

In summary, by using organic dyes, rather than emissive nanostructures, as the probes, we have demonstrated that MnO_2 nanosheets-suppressed fluorescence emission can be used as a new sensing platform with excellent analytical properties. With the organic dyes as the probes, the suppressive effects of MnO_2 nanosheets on the fluorescence of the organic dyes can be easily manipulated through multiple and even tailor-made mechanisms by rationally choosing dyes and thereby tuning the interactions between MnO_2 nanosheets with different sorts of dyes. Moreover, the use of the organic dyes as the probes would largely enable the selectivity to be easily achieved for the sensing platform. This study essentially offers a new 2D nanostructure-based fluorescent sensing platform, which is robust, technically simple, and easily manipulated to achieve high selectivity and sensitivity for various applications.

Acknowledgements

This work was financially supported by the National Natural Science Foundation of China (Grant Nos. 21321003, 21210007, and 91213305 for L. Mao; 21322503 for P. Yu), and the National Basic Research Program of China (973 programs, 2013CB933704).

References

1 Z. L. Zhao, H. H. Fan, G. F. Zhou, H. R. Bai, H. Liang, R.W. Wang, X. B. Zhang and W. H. Tan, *J. Am. Chem. Soc.*, 2014, **136**, 11220-11223.

2 Y. Chen, C. L. Tan, H. Zhang and L. Z. Wang, *Chem. Soc. Rev.*, DOI: 10.1039/C4CS00300D.

3 C. F. Zhu, Z. Y. Zeng, H. Li, F. Li, C. H. Fan and H. Zhang, *J. Am. Chem. Soc.*, 2013, **135**, 5998-6001.

4 Y. X. Yuan, R. Q. Li and Z. H. Liu, *Anal. Chem.*, 2014, **86**, 3610-3615.

5 C. K. Wu, Y. M. Zhou, X. M. Miao and L. S. Ling, *Analyst*, 2011, **136**, 2106-2110

6 X. H. Zhao, R. M. Kong, X. B. Zhang, H. M. Meng, W. N. Liu, W. H. Tan, G. L. Shen and R. Q. Yu, *Anal. Chem.*, 2011, **83**, 5062-5066.

7 Z. B. Liu, S. S. Chen, B. W. Liu, J. P. Wu, Y. B. Zhou, L. Y. He, J. S. Ding and J. W. Liu, *Anal. Chem.*, 2014, **86**, 12229-12235.

8 Y. P. Wang, Y. H. Xiao, X. L. Ma, N. Li and X. D. Yang, *Chem. Commun.*, 2012, **48**, 738-740.

9 C. H. Lu, H. H. Yang, C. L. Zhu, X. Chen and G. N. Chen, *Angew. Chem. Int. Ed.*, 2009, **48**, 4785-4787.

10 S. J. He, B. Song, D. Li, C. F. Zhu, W. P. Qi, Y. Q. Wen, L. H. Wang, S. P. Song, H. P. Fang and C. H. Fan, *Adv. Funct. Mater.*, 2010, **20**, 453-459.

11 Q. B. Wang, W. Wang, J. P. Lei, N. Xu, F. L. Gao and H. X. Ju, *Anal. Chem.*, 2013, **85**, 12182-12188.

12 B. A. Pinaud, Z. B. Chen, D. N. Abram and T. F. Jaramillo, *J. Phys. Chem. C*, 2011, **115**, 11830-11838.

13 Y. Omomo, T. Sasaki, L. Z. Wang and M. Watanabe, *J. Am. Chem. Soc.*, 2003, **125**, 3568-3575.

14 K. Kai, Y. Yoshida, H. Kageyama, G. Saito, T. Ishigaki, Y. Furukawa and J. Kawamata, *J. Am. Chem. Soc.*, 2008, **130**, 15938-15943.

15 L. L. Peng, X. Peng, B. R. Liu, C. Z. Wu, Y. Xie and G. H. Yu, *Nano Lett.*, 2013, **13**, 2151-2157.

16 M. Toupin, T. Brousse and D. Bélanger, *Chem. Mater.*, 2004, **16**, 3184-3190.

17 S. H. Yang, X. F. Song, P. Zhang and L. Gao, *ACS Appl. Mater. Interfaces*, 2013, **5**, 3317-3322.

18 R. R. Deng, X. J. Xie, M. Vendrell, Y.-T. Chang and X. G. Liu, *J. Am. Chem. Soc.*, 2011, **133**, 20168-20171.

19 X. L. Zhang, C. Zheng, S. S. Guo, J. Li, H. H. Yang and G. N. Chen, *Anal. Chem.*, 2014, **86**, 3426-3434.

20 Y. X. Yuan, S. F. Wu, F. Shu and Z. H. Liu, *Chem. Commun.*, 2014, **50**, 1095-1097.

21 W. Y. Zhai, C. X. Wang, P. Yu, Y. X. Wang and L. Q. Mao, *Anal. Chem.*, 2014, **86**, 12206-12213.

22 I. Dilek, M. Madrid, R. Singh, C. P. Urrea and B. A. Armitage, *J. Am. Chem. Soc.*, 2005, **127**, 3339-3345.

23 A. L. Benvin, Y. Creeger, G. W. Fisher, B. Ballou, A. S. Waggoner and B. A. Armitage, *J. Am. Chem. Soc.*, 2007, **129**, 2025-2034.

24 H. F. Dong, W. C. Gao, F. Yan, H. X. Ji and H. X. Ju, *Anal. Chem.*, 2010, **82**, 5511-5517.

25 T. D. Gauthier, E. C. Shane, W. F. Guerin, W. R. Seltz and C. L. Grant, *Environ. Sci. Technol.*, 1986, **20**, 1162-1166.

26 J. Q. Tian, N. Y. Cheng, Q. Liu, W. Xing and X. P. Sun, *Angew. Chem. Int. Ed.*, DOI: 10.1002/anie.201501237.

27 H. L. Li, Y. W. Zhang, Y. L. Luo and X. P. Sun, *Small*, 2011, **7**, 1562-1568.

28 L. Wang, Y. W. Zhang, J. Q. Tian, H. L. Li and X. P. Sun, *Nucleic Acids Res.*, 2011, **39**, e37.

29 H. L. Li, Y. W. Zhang, L. Wang, J. Q. Tian, and X. P. Sun, *Chem. Commun.*, 2011, **47**, 961-963.

30 H. L. Li and X. P. Sun, *Chem. Commun.*, 2011, **47**, 2625-2627.

31 S. Liu, L. Wang, Y. L. Luo, J. Q. Tian, H. L. Li and X. P. Sun, *Nanoscale*, 2011, **3**, 967-969.

32 S. Guo, D. X. Du, L. N. Tang, Y. Ning, Q. F. Yao, and G. J. Zhang, *Analyst*, 2013, **138**, 3216-3220.

33 I. Nazarenko, R. Pires, B. Lowe, M. Obaidy and A. Rashtchian, *Nucleic Acids Res.*, 2002, **30**, 2089-2195.

34 K. K. Farh, A. Grimson, C. Jan, B. P. Lewis, W. K. Johnston, L. P. Lim, C. B. Burge, and D. P. Bartel, *Science*, 2005, **310**, 1817-1821.

35 C. Arenz, *Angew. Chem. Int. Ed.*, 2006, **45**, 5048-5050.

36 J. Lu, G. Getz, E. A. Miska, E. Alvarez-Saavedra, J. Lamb, D. Peck, A. Sweet-Cordero, B. L. Ebert, R. H. Mak, A. A. Ferrando, J. R. Downing, T. Jacks, H. R. Horvitz, T. R. Golub, *Nature*, 2005, **435**, 834-841.

37 K. A. Cissell, S. Shrestha and S. K. Deo, *Anal. Chem.*, 2007, **79**, 4754-4761.

38 D. P. Bartel, *Cell*, 2004, **116**, 281-297.

39 L. He and G. J. Hannon, *Nat. Rev. Genet.*, 2004, **5**, 522-531.

40 H. Dong, J. P. Lei, L. Ding, Y. Q. Wen, H. X. Ju and X. J. Zhang, *Chem. Rev.*, 2013, **113**, 6207-6233.

41 R. Sanuki, A. Onishi, C. Koike, R. Muramatsu, S. Watanabe, Y. Muranishi, S. Irie, S. Uneo, T. Koyasu, R. Matsui, Y. Chérasse, Y. Urade, D. Watanabe, M. Kondo, T.

Yamashita and T. Furukawa, *Nat. Neurosci.*, 2011, **14**, 1125-1134.

42 R. Saba and S. A. Booth, *BMC Biotechnology*, 2006, **6**: 47.

43 M. Lagos-Quintana, R. Rauhut, A. Yalcin, J. Meyer, W. Lendeckel and T. Tuschil, *Curr. Biol.*, 2002, **12**, 735-739.

44 Y. Q. Cheng, X. Zhang, Z. P. Li, X. X. Jiao, Y. C. Wang and Y. L. Zhang, *Angew. Chem. Int. Ed.*, 2009, **48**, 3268-3272.

45 H. F. Dong, J. Zhang, H. X. Ju, H. T. Lu, S. Y. Wang, S. Jin, K. H. Hao, H. W. Du and X. J. Zhang, X. *Anal. Chem.*, 2012, **84**, 4587-4593.

46 H. Y. Liu, L. Li, Q. Wang, L. L. Duan and B. Tang, *Anal. Chem.*, 2014, **86**, 5487-5493.

47 Q. Xi, D. M. Zhou, Y. Y. Kan, J. Ge, Z. K. Wu, R. Q. Yu, and J. H. Jiang, *Anal. Chem.*, 2014, **86**, 1361-1365.

48 T. Tian, H. Xiao, X. L. Zhang, S. Peng, X. E. Zhang, S. Guo, S. R. Wang, S. M. Liu, X. Zhou, C. Meyers and X. Zhou, *Chem. Commun.*, 2013, **49**, 75-77.

49 L. Cui, X. Y. Lin, N. H. Lin, Y. L. Song, Z. Zhu, X. Chen and C. Y. Yang, *Chem. Commun.*, 2012, **48**, 194-196.

50 Y. Sato, Y. Toriyabe, S. Nishizawa and N. Teramae, *Chem. Commun.*, 2013, **49**, 9983-9985.

51 J. Ruta, S. Perrier, C. Ravelet, J. Fize and E. Peyrin, *Anal. Chem.*, 2009, **81**, 7468-7473.

52 A. Bini, M. Minunni, S. Tombelli, S. Centi and M. Mascini, *Anal. Chem.*, 2007, **79**, 3016-3019.

53 Y. H. Wang, L. Bao, Z. H. Liu and D. W. Pang, *Anal. Chem.*, 2011, **83**, 8130-8137.

For TOC